SMAR 2017 – Fourth Conference on Smart Monitoring,
Assessment and Rehabilitation of Civil Structures

SMAR 2017

Numerical simulations of medium and high frequency elastic waves for damage detection in composite wind turbine blades

Filip Szlaszyński[1] and Piotr Omenzetter[2]

[1] The University of Aberdeen, Aberdeen, UK
[2] The Lloyd's Register Foundation Centre for Safety and Reliability Engineering, The University of Aberdeen, Aberdeen, UK

ABSTRACT: This paper numerically investigates the phenomenon of elastic wave (EW) propagation in large composite wind turbine blades and its suitability for damage detection. The study is performed using ANSYS® Mechanical finite element software on the model of NREL offshore 5MW baseline wind turbine blade. The source of elastic waves is a surface impact generating a broadband elastic wave pulse. The motion of elastic waves is illustrated in surface deformation plots and the key observations such as wave reflection, interference and scattering are addressed in discussion. The research also examines the interaction of the introduced waves with a surface crack perpendicular to the direction of wave propagation. It is concluded that medium and high frequency EWs have much higher sensitivity to this type of damage in comparison to low frequency EWs, and are argued to have a good potential for damage detection.

1 INTRODUCTION

Amongst all the renewable energy sources available for exploitation, wind power stands out as the one whose utilisation is the fastest growing in the world. Wind is an ample, pollution-free and safe source of energy. Over the past 30 years, wind turbines (WTs) have significantly increased in size to improve their efficiency and to increase the amount of energy harvestable by a single device. The increased capabilities came at a price of greater complexity, higher likelihood of failure and more frequent maintenance (Jin et al., 2016). Moreover, WTs are placed in more remote and inaccessible locations, such as offshore areas, where on-site inspections are costly, require shut-downs and can only be performed under good weather conditions.

Currently, the economics of offshore wind energy is less favourable than the onshore energy, therefore the significant cost reduction is needed for it to become competitive with fossil fuel energy. Since the initial investment accounts for about 70% of the produced offshore electricity cost, the substantial reduction in price per megawatt of energy can be obtained by extending the service life of WTs, increasing their safety and reliability by limiting the number of costly on-site inspections (Junginger et al., 2004). These objectives could be achieved by deployment of automated structural health monitoring (SHM) systems capable of continuous, real-time and remote monitoring of structural condition of WTs. At present, the development of such robust systems capable of damage detection in large composite WTs is the objective of many studies around the world. The focus is on wind turbine blades (WTBs) as the most critical components with the highest risk of failure and accounting for 15–20% of the total cost of a WT (Yang et al., 2016).

Currently, many the most promising techniques for SHM of composite WTBs use EW propagation. The EW are time-varying deformations (vibrations) in material, propagating in an elastic medium as a result of forces associated with volume deformation (compression and extension) and shape deformation (shear) of medium elements (Ostachowicz et al., 2012). There are different types of EWs that can be classified based on the direction of particle motion in relation to direction of elastic wave propagation (Ostachowicz et al., 2013). The type of EWs occurring in each case mainly depends on boundary conditions (restrictions) imposed on the elastic medium and material thickness in relation to wave length.

In an unlimited three-dimensional solid body, the so-called bulk waves occur. One can distinguish two types of bulk waves. The longitudinal, whose particle motion is in the direction of wave propagation, and the shear waves with the particle motion in the direction perpendicular to wave propagation (Ostachowicz et al., 2013). If the medium is bounded with one surface, the Rayleigh and Love surface waves occur (Ostachowicz et al., 2012). The particle motion in these waves is more complex than in two previous types and its amplitude decrease with material depth.

In a case of elastic body bounded with two surfaces (e.g. a WTB shell), the longitudinal waves and shear waves propagate simultaneously interacting with each other and creating a new type of EWs called Lamb waves. Depending on the distribution of displacements on the top and bottom of the bounding surface, these waves exist as infinite number of symmetrical and antisymmetrical modes (Ostachowicz et al., 2012). Although, the number of these modes is infinite, the number of propagating modes depends on the product of the excitation frequency and material thickness (Ostachowicz et al., 2013). The Lamb waves are of a particular interest in non-destructive testing and SHM of WTB as blades are made of shell-like and plate-like elements in which Lamb waves are the dominant type of waves.

The suitability of EWs for SHM systems comes from the fact that wave propagating through the medium interacts with material discontinuities on its way. The discontinuity can be an edge or stiffening element, but it can also be damage site. An EW encountering the discontinuity reflects and/or refracts, often with change in its characteristics (the mode, phase, amplitude, wave length etc.). Therefore, the waves reflected and refracted from defects carry information on the type, location and size of damage. By recording and analysing these waves this information can be extracted (Ostachowicz et al., 2012) and used for SHM.

This paper investigates numerically the propagation of impact-induced surface EWs. The impact type load was chosen for this study as it is the simplest method of inducing traveling EWs in a solid body, producing a distinctive primary wave front whose behaviour over time can easily be observed in plots of the deformed surface. Application of this type of loading to SHM of composite WTBs was experimentally investigated by Tcherniak and Mølgaard (2015).

2 FINITE ELEMENT ANALYSIS OF IMPACT-INDUCED ELASTIC WAVES

2.1 Finite element model

This study is based on numerical model of a large composite WTB. The blade is a part of the National Renewable Energy Laboratory (NREL) offshore 5MW baseline wind turbine used in numerous studies including the aerodynamics, controls, offshore dynamics and design code development. The WT has a rotor diameter of 126 m and a hub height of 90 m which matches the current developments of the onshore and offshore WTs. The WTB is 61.5m long and weighs 17,740kg. The blade structural design meets the design criteria set by International Electrotechnical Committee (IEC, 2015) standards for the onshore version of this turbine. The

model, which is described in detail in Resor (2013), was deemed accurate enough for research applications – for example it was used in Hoell and Omenzetter (2016) and many other investigations.

The baseline finite element (FE) model of the WTB was created using ANSYS® Mechanical and NuMAD software tool provided by Sandia National Laboratories. ANSYS® was chosen because of its common usage in the wind industry and its strong capabilities to create the blade geometry. It is meshed with 2D quadrilateral-shaped elements (area mesh). The quadrilateral elements are preferred to triangular as they provide better control of the mesh and reduce numerical error. The quadrilateral elements create a structured grid which has lower skewness, better convergence, and higher resolution than an unstructured grid. Additionally, the structure grid model is highly space efficient.

Among the quadrilateral elements, two structural shell elements with six kinematic degrees of freedom (DOFs) per node were considered, i.e. the ANSYS® SHELL181 (four nodes) and SHELL281 elements (eight nodes). The SHELL281 elements were chosen based on element type and mesh size study done by Hoell (2016). The investigated FE model consists of 18,769 elements, 55,095 nodes and approximately 324,700 DOFs. Cantilever-type boundary conditions are introduced by fixing all DOFs at the blade root, thus the WT tower and hub flexibilities are ignored in the study.

2.2 Wave propagation phenomenon captured by FE simulations

The propagation of EWs is a transient phenomenon. The transient analysis was performed using ANSYS® Academic software over a period of 0.2 seconds. The nodal displacements and accelerations were calculated for 2,000 intermediate time steps. The simulation set up is presented in Figure 1. The impact loading of magnitude of 100N was applied to the node at the surface of the blade model at its centre (between the structural shear webs), at approximately 1/5 of the WTB length from its root. The impact loading was imitated by a triangular function applied for 0.0002s as proposed in Madenci and Guven (2006). The function is presented in Figure 2. The displacements and accelerations were calculated for points S1-S6 lying on the central axis of WTB on the upper and lower surfaces.

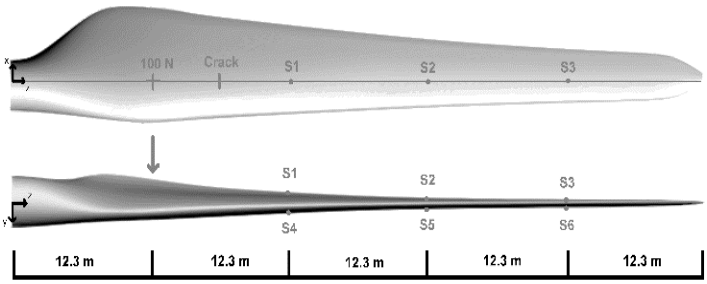

Figure 1: Simulation set-up.

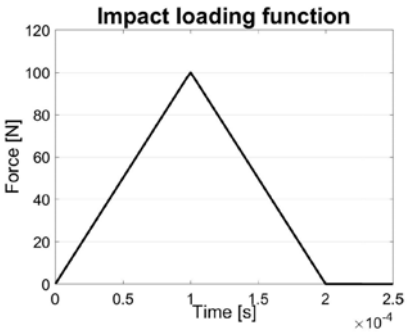

Figure 2: Impact function.

The displacements are captured in a series of slides presented in Figure 3. It can be seen that an impact produced a circular deformation around the point of application of the force. The deformation propagated outwards of its origin as a wave front. Behind the first wave front, the

secondary wave fronts of smaller amplitudes occurred. The observed phenomenon is the consequence of the Huygens principle stating, that the wave front is the envelope of the wavelets. Each point on a wave front acts as an independent source of wavelets for the next wave front (Mathpages.com, 2017), which occurs at the line tangent to all the new wavelets. Therefore, the initial wave front created by an impact is followed by secondary wave fronts. Each of the secondary wave fronts has a lower amplitude as the energy is being spread over larger area as the wave propagates. However, as mentioned in many studies, (i.e. Perton and Sánchez-Sesma, 2015), application of this principle to surface EWs is more complex and requires taking into consideration the coexistence of different types of elastic waves, differences in their characteristics (e.g. a longitudinal and a transverse wave propagate at different speeds, the trajectory of their motion is different etc.), and effects related to the non-homogeneity of composite material. This paper does not delve into analytical consideration of the phenomenon; it only provides illustration of the process for better understanding of simple principles of EWs propagation in complex structures.

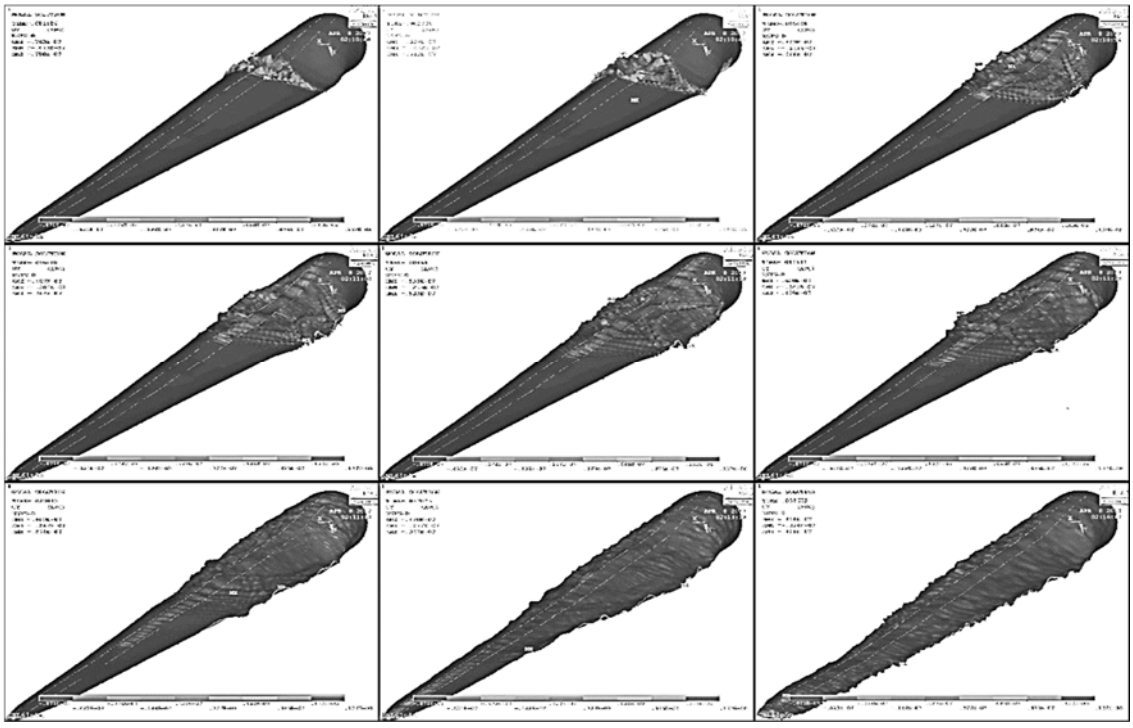

Figure 3: Animation of EW propagation in a composite WTB (snapshots taken between 0.0019s and 0.0114s after an impact was applied).

As the impact-introduced wave fronts propagate through the WTB, they encounter boundaries of the body. It can be clearly seen in the 3rd and 4th slide in Figure 3 how the waves reflect from the blade trailing and leading edges and the reflected EWs travel in the opposite directions to the incident ones. Constructive interference of the waves can be observed in the 5th slide, when the crests of reflected waves meet the crests of the wave fronts traveling towards the blade tip. On the other hand, destructive interference can be seen in the 6th slide, where the waves reflected from the trailing edge meet the ones reflected from the leading edge. The EW amplitudes suddenly decrease, they scatter and one cannot identify distinct wave fronts any more. This phenomenon is also partially associated with the presence of stiffening shear webs beneath the blade surface

(marked with two thin white lines along the length of the blade at its central part). As the time passes the initial wave front reaches the blade tip and reflects from its edge, as can be seen in the 7th, 8th and 9th slide. The reflected waves interfere with the secondary wave fronts traveling towards the tip. EW scattering occurs, resulting in small rotations of the blade tip.

2.3 Displacements and accelerations of blade surface

The time-history plots of displacements and accelerations in the direction perpendicular to the blade surface were obtained from the simulation discussed in the previous section. In the displacement plots (Figure 4) for points S1, S3 and S4 (shown in Figure 1), the ragged curves indicate that EWs introduced by an impact comprise multiple frequencies imposed on each other. This was confirmed by a single-sided spectral analysis obtained by performing the fast Fourier transform (FFT) on the displacement results over the simulated period using build-in function in MATLAB® software. The observation agrees with experimental findings of Tcherniak and Mølgaard (2015). (A plot of amplitude spectra at point S1 is presented later in Figure 8.)

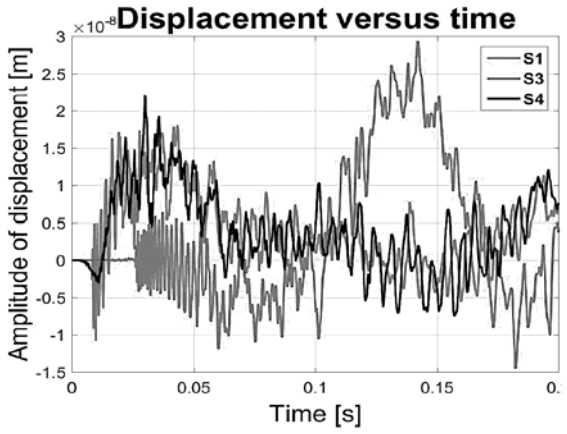

Figure 4: Displacement time history for points S1, S3 and S4.

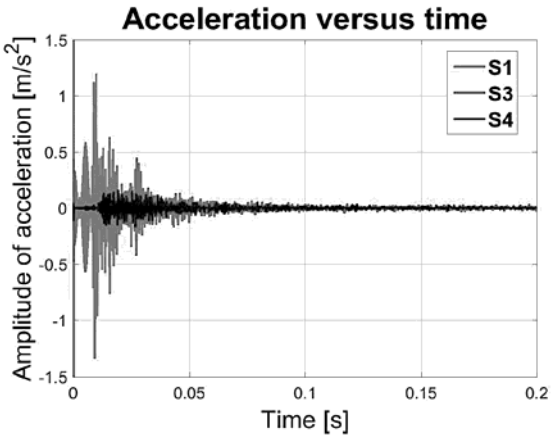

Figure 5: Acceleration time history for points S1, S3 and S4.

The displacement plot in Figure 4 also shows large fluctuations in displacements amplitude at all the considered points after an arrival of the initial wave front. For example, at point S3, the surface wave front arrives around 0.03 seconds after the impact and has an amplitude of 0.5×10^{-8} m, then from 0.1 seconds after the impact the amplitude of displacement start rising to finally reach almost 3×10^{-8} m at 0.14 seconds. The reason for that are the low frequency structural vibrations of the entire WTB induced by the impact. They have amplitudes and wave lengths several times larger than the surface EWs. The low frequency EWs are generally known to be insensitive to small damage, therefore are of limited use in SHM of WTBs. However, their co-occurrence makes it more difficult to extract information about the damage from the higher frequency EWs. However, a simple solution for this problem is to measure accelerations instead of displacements. For higher frequencies, the crest-trough transition is very fast, resulting in high accelerations, whereas for low frequencies the transition is slow and the accelerations are low. Therefore, the contribution of low vibrations to acceleration spectrum is relatively small as can be seen in Figure 5. On the other hand, in practical applications noise at higher frequencies may be an issue.

It is worth noticing, that the amplitude of the aforementioned low frequency vibrations is larger near the WTB tip (point S3). This is caused by the cantilever boundary conditions imposed in the model.

The amplitude of vibrations on the opposite side of the WTB to the applied force is almost identical to the one on the impacted side at the corresponding points (i.e. S1 and S4). However, the amplitude of accelerations is much smaller, and the spectral analysis using FFT revealed slightly higher magnitudes of very low frequencies on the opposite side to forcing, and much lower magnitudes for frequencies higher than 200 Hz. Therefore, it can be concluded that structural shear webs transfer low frequencies well to the other side of the blade, however they perform worse at transferring medium and high frequencies.

2.4 Damage-wave interactions

The damage-EW interaction study was performed on the FE model. The surface crack was chosen to be investigated as its effect on the surface EWs can be clearly illustrated on the surface deformation plots. The simulation has also a real world relevance, as the occurrence of the surface cracks during WTs operation was observed in the study performed by Ataya and Ahmed (2011).

Damage in a form of surface crack perpendicular to the length of blade was introduced around 18.5 m from the WTB root, between the applied force and point S1, as shown in Figure 6. It was artificially imitated in the FE model by removal of couplings between the nodes of the adjacent elements as proposed by Hoell (2016). Doing so resulted in a lack of connection between the elements on a length of around 80 cm.

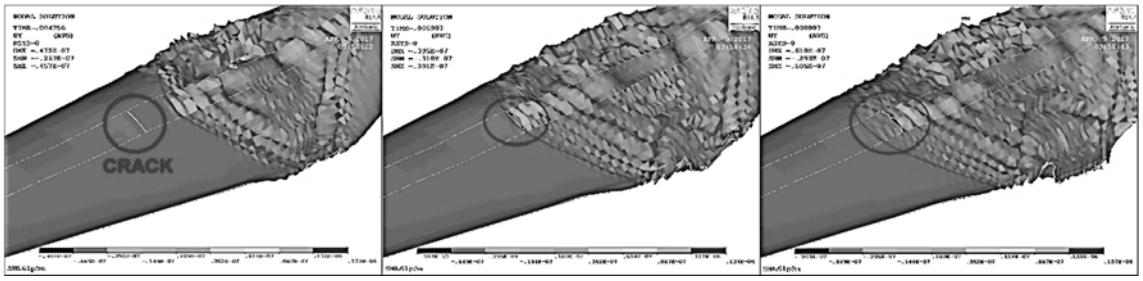

Figure 6: EW – crack interaction (snapshots taken at approx. 0.0048s, 0.0069s and 0.0080s after an impact).

The animation of the EWs traveling after an impact is presented in Figure 6. When the incident wave front arrives at the crack, the part that is in contact with damage is reflected, whereas the part traveling over undamaged surface propagates further. The surface immediately after the crack is excited by adjacent waves, which did not interfere with damage, in accordance with the Huygens principle mentioned earlier. The amplitude of the deformations behind the crack is much lower comparing to the case where crack was not present.

The time history of the displacements at points S1-S6 was compared between undamaged and damaged states in Figure 7. The notable alteration of the EWs due to the surface damage was only experienced at 3 points (S1, S2 and S3), which were located on the same side of the blade as the damage and forcing. At the points on the other side (S4, S5 and S6) of the blade, the change of wave amplitudes of displacements was very small – possibly too small to be captured in actual measurements. A comparative plot of the deformation time histories at point S1 for both states is presented in Figure 8. It can be observed that the amplitudes of the initial wave front re much smaller when damage is present, however, as the time passes the amplitudes of EWs for both

conditions start to coincide. It can be concluded that only the initial wave front is significantly affected by the crack. Once the area immediately after the crack is set in motion, it behaves almost identical as if no crack were present.

Spectral plots for the undamaged and damaged states are plotted for point S1 in Figure 8. It can be noted that lower frequencies are very little affected by the crack, therefore their sensitivity to these type of damage is very low. On the other hand, the magnitudes of the medium and high frequencies are significantly altered by the crack existence, thus they may be suitable for damage detection. A comparison of phase plots between the displacement time histories in the undamaged and damaged states, presented in Figure 9, indicates that damage does also cause phase shifts. The highest phase shifts are observed at high frequencies in the range of 2 kHz and 8 kHz and they could also be used for damage detection.

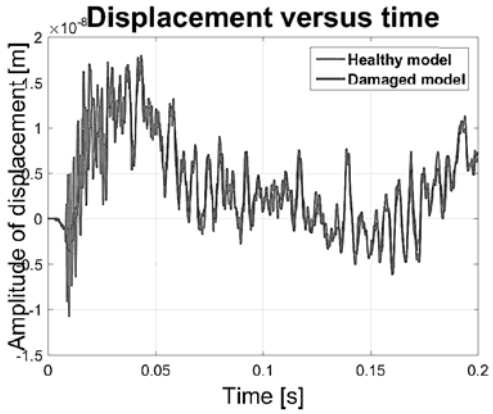

Figure 7: Displacement time histories for baseline and damaged states at point S1.

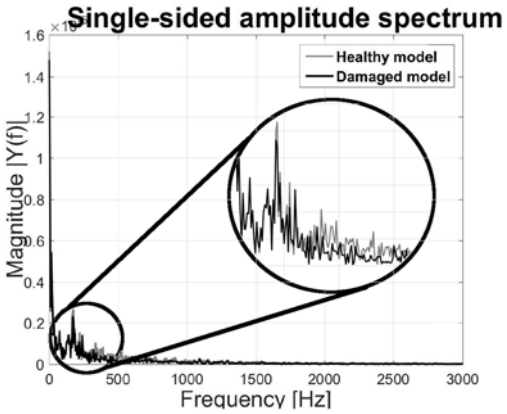

Figure 8: Single-sided amplitude spectra for baseline and damaged states at point S1.

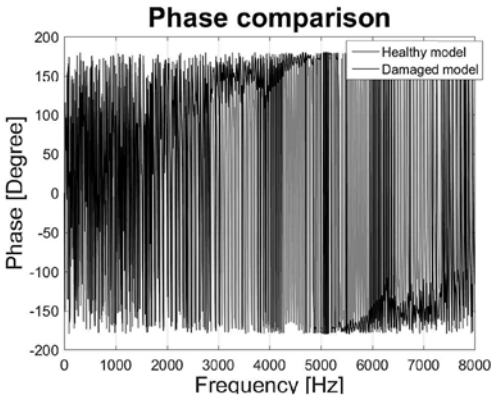

Figure 9: Phases of displacements in baseline and damaged states at point S1.

3 CONCLUSIONS

The research investigated the propagation of EWs induced by surface impact in large composite WTBs. It can be concluded that surface impact produces EWs of a wide range of frequencies propagating as wave fronts. The character of surface motion in points along the blade changes in time as waves interact with the boundaries of a body, stiffening elements and other elastic waves.

Reflections, constructive and destructive interferences and scattering alter the EW profiles over time. The study revealed that medium and high frequencies have a better potential for damage detection applications. Low frequencies have low sensitivity for small discontinuities in the structure (i.e. cracks). A crack perpendicular to direction of the wave propagation causes reflection of the medium and high frequency EWs as was shown in the surface deformation animation snapshots. This results in an alteration of surface motion profiles, namely the attenuation of displacement magnitudes behind the damage and phase changes. The existence of EWs immediately behind a crack was observed to be induced by the adjacent waves traveling over undamaged areas. Furthermore, it was noted that the incident wave front characteristics are more affected by the crack presence than the secondary wave fronts. Finally, it can be concluded that impact-based SHM system could be used for active damage detection as it introduces the wide range of frequencies, including the desired medium and high frequencies.

4 REFERENCES

Ataya, S. and Ahmed, M. M. Z. (2011). Forms of discontinuities in 100 kW and 300 kW wind turbine blades. Proc. 10th World Wind Energy Conference & Renewable Energy Exhibition, 1–6, Cairo, Egypt.

Hoell, S. (2016). Optimal feature projections for enhanced vibration-based damage identification with an application to wind turbine blades. Ph.D. thesis, University of Aberdeen.

Hoell, S. and Omenzetter, P. (2016). Optimal selection of autoregressive model coefficients for damage detectability with an application to wind turbine blades. Mechanical Systems and Signal Processing, 70-71, 557–577.

International Electrotechnical Committee (IEC). (2005). Wind turbines – Part 1: Design requirements. 3 ed. Geneva: International Electrotechnical Committee.

Jin, X., Gan, Y., Ju, W., Yang, X. and Han, H. (2016). Research on wind turbine safety analysis: Failure analysis, reliability analysis, and risk assessment. Environmental Progress & Sustainable Energy, 35(6), 1848-1861.

Junginger, M., Faaij, A. and Turkenburg, W. (2004). Cost reduction prospects for offshore wind farms. Wind Engineering, 28(1), 97-118.

Madenci, E. and Guven, I. (2006). The finite element method and applications in engineering using ANSYS®. 1st ed. New York: Springer, 460-461.

Mathpages.com. (2017). MathPages. Available at: www.mathpages.com [Accessed 12 Apr. 2017].

Ostachowicz, W., Kudela, P., Krawczuk, M. and Zak, A. (2012). Guided waves in structures for SHM: The time - domain spectral element method. 2nd ed. Chichester: Wiley.

Ostachowicz, W., Malinowski, P. and Wandowski, T. (2013). Damage localisation using elastic waves propagation method. Experimental techniques. In: W. Ostachowicz and A. J. Güemes, eds. New trends in structural health monitoring. Vienna: Springer, 317-371.

Perton, M. and Sánchez-Sesma, F. (2015). The indirect boundary element method to simulate elastic wave propagation in a 2-D piecewise homogeneous domain. Geophysical Journal International, 202(3), 1760-1769.

Resor, B. R. (2013). Definition of a 5MW/61.5m wind turbine blade reference model, Albuquerque, New Mexico: Sandia National Laboratories.

Tcherniak, D. and Mølgaard, L. L. (2015). Vibration-based SHM system: Application to wind turbine blades. Journal of Physics, 628.

Yang, R., He, Y. and Zhang, H. (2016). Progress and trends in nondestructive testing and evaluation for wind turbine composite blades. Renewable and Sustainable Energy Reviews, 60, 1225-1250.